frontiers | Frontiers in Materials

ORIGINAL RESEARCH
published: 08 April 2022
doi: 10.3389/fmats.2022.878682

One-Pot Fabrication of Poly (Ionic Liquid)/TiO_2 Composite as an Electrorheological Material With Enhanced Electro-Responsive Properties and Broader Operation Temperature Range

*Guangchen Zhang, Shu Yang, Zhenjie Zhao, Chenjie Dong, Xiao Jin, Li-Min Wang and Ying Dan Liu**

State Key Lab of Metastable Materials Science and Technology, College of Materials Science and Engineering, Yanshan University, Qinhuangdao, China

OPEN ACCESS

Edited by:
Qingyu Peng,
Harbin Institute of Technology, China

Reviewed by:
Jinbo Wu,
Shanghai University, China
Xufeng Dong,
Dalian University of Technology, China
Jie Fu,
Chongqing University, China

***Correspondence:**
Ying Dan Liu
ydliu@ysu.edu.cn

Specialty section:
This article was submitted to Smart Materials, a section of the journal Frontiers in Materials

Received: *18 February 2022*
Accepted: *08 March 2022*
Published: *08 April 2022*

Citation:
Zhang G, Yang S, Zhao Z, Dong C, Jin X, Wang L-M and Liu YD (2022) One-Pot Fabrication of Poly (Ionic Liquid)/TiO_2 Composite as an Electrorheological Material With Enhanced Electro-Responsive Properties and Broader Operation Temperature Range. Front. Mater. 9:878682. doi: 10.3389/fmats.2022.878682

Poly (ionic liquid)/TiO_2 composite particles were fabricated using a facile one-pot synthesis method, in which the polymerization of the ionic liquid monomer and hydrolysis of the precursor for TiO_2 proceeded in one system. The morphological properties of the composite particles were observed by a scanning electron microscope and transmission electron microscope. The chemical and physical structures of the particles were analyzed by a Fourier infrared spectrometer and an X-ray diffractometer, respectively. It was found that in the composite particles, poly (ionic liquid) (PIL) spheres are embedded in the continuous TiO_2 phase, forming larger nonspherical particles of ~10 microns. The rheological properties of PIL and the PIL/TiO_2 composite particles dispersed in silicone oil were measured by a rotational rheometer with a high-power supply. At the same electric field, the PIL/TiO_2 particles showed higher shear stress and elastic modulus than pure PIL particles at the same electric field. In addition, compared with pure PIL particles, the PIL/TiO_2 particles work at higher temperatures, up to 100°C.

Keywords: electrorheological fluid, poly (ionic liquid), TiO_2, composite, one-pot fabrication

INTRODUCTION

Electrorheological (ER) fluids (Halsey, 1992) are a kind of intelligent suspension comprising electrically polarizable particles of nano-to-micron size and insulating oil. The particles in the suspension can construct chain structures from a disordered dispersion state in milliseconds under the stimulation of an electric field, which increases the viscosity of the system enormously and makes the ER fluids perform like solids. This liquid-to-solid transition is fast, reversible, and controllable. These characteristics of ER fluids show broad application potential in various mechanical devices with flexible controllability, such as damping shock absorbers (Bitman et al., 2004; Sun et al., 2020), clutches (Kikuchi et al., 2020), ultra-precision processing machines (Zhao et al., 2021), lubrication systems (Delgado-Canto et al., 2020; Agrawal and Shama, 2021), and tactile displays (Liu et al., 2005; Chen et al., 2020).

Related studies have found that the intelligent characteristics of ER fluids, such as yield stress, zero-field viscosity, and response time, are mainly attributed to the dispersion and interaction of electro-polarized particles in the fluid under the action of an electric field (Hao et al., 1997; Liang et al., 2020). The dispersed particles of ER fluids, also known as ER materials, can be divided into inorganics, organics, and organic–inorganic composites. In terms of inorganic ER materials, most research has been carried out on titanium dioxide (TiO_2) and perovskite nanomaterials (Zhao and Yin, 2002; Wu et al., 2016; Sun et al., 2021). By means of doping, the design of special morphologies and modification by polar molecules, titanium oxide hybrid inorganics display giant ER effects with high yield stress up to 100 kPa (Wen et al., 2003; Qiu et al., 2019). Other 2D and 3D inorganic materials such as graphene, MoS_2, and Mxenes have also been applied as ER materials; however, expected outstanding ER effects have not been revealed in these materials (Zhang and Choi, 2014; Lee et al., 2016; Zhang et al., 2019). In the research of inorganic ER materials, distinct defects were discovered, which included poor dispersion stability and abrasion to devices. By contrast, organic ER materials can overcome the defects of inorganics attributed to their soft structure and low density. Conductive polymers (Plachy et al., 2015; Lu et al., 2018), biopolymers (Liu et al., 2018; Kovaleva et al., 2022), and polyelectrolytes (Schwarz et al., 2013) are the most concerned candidates as organic ER materials. Although organic ER materials can overcome some shortcomings of inorganic materials, they have no major breakthrough in yield stress, and their thermal stability is not as good as that of inorganic materials. Therefore, inorganic/organic hybrid materials combining the advantages of inorganics and organics have attracted considerable attention in recent research on ER materials (Jang et al., 2019; Wen et al., 2019).

It is worth noting that a special organic, ionic liquid (IL) has been introduced to prepare ER materials (Marins, et al., 2013; Zhao et al., 2020). It is a kind of organic salt comprising anions and cations with mismatched sizes and remains liquid at room temperature (Martyn and Kenneth, 2020). Most IL molecules have the advantages of high conductivity, excellent thermal stability, low vapor pressure, and diverse structures that can be designed (Armand et al., 2009; Gao et al., 2017). In contrast to their application in electrolytes, the ions of IL molecules as ER materials are not allowed to move freely to prevent the appearance of short circuits in electric fields. Therefore, poly (ionic liquid) (PIL) (Dong et al., 2014; Zhang, et al., 2017) and IL-modified inorganics (Zhang et al., 2021) are fabricated to reduce the conductivity and maintain most of the original properties of the IL at the same time. PIL-based ER materials have been intensively studied by Yin et al. It was found that the ER effect of PIL was closely related to the chemical structures of cations and anions and the molecular weight of the PIL (Zhao et al., 2019; He et al., 2021; Liu et al., 2019b). The ER effect of the PIL can be adjusted flexibly by varying the chemical structures of the PIL. Unfortunately, pure PIL with a low glass transition temperature limits the operating temperature of ER fluids (Liu et al., 2019a). Designing composite structures with inorganics is an effective way to improve the stability of PIL-based ER materials at higher temperature. However, most procedures for preparing composite particles are relatively complicated (Lei et al., 2018; Zhao et al., 2018). A facile fabrication method for PIL-based composite materials is necessary to study their electroresponsive properties and wide application characteristics further.

In this study, we fabricated PIL/TiO_2 composite particles using a one-pot synthesis method. The composite particles combined the high dielectric TiO_2 with the soft, versatile PIL. In the one-pot method, the polymerization of the IL monomer and the sol–gel process of TiO_2 occurred in one system. The two kinds of chemical interactions influenced each other in the synthesis process such that the morphologies of the PIL/TiO_2 particles are very different from those of spherical PIL particles. The structures and ER properties of the PIL/TiO_2 particles were analyzed and compared with those of pure PIL particles. Rheological analysis indicated that the PIL/TiO_2 composite particles showed enhanced ER effect and excellent ER stability at higher temperature up to 100°C.

MATERIALS AND METHODS

Materials

Titanium isopropoxide (TTIP) (97%, MACKLIN), 1-vinyl-3-butylimidazolium tetrafluoroborate ([VBIm][BF_4]) (99%, Lanzhou Greenchem ILs), polyvinyl pyrrolidone (PVP) (K90, AR, Sigma-Aldrich), and ethanol (AR, Tianjin Kaitong Chemical Reagent Co. Ltd.) were used without additional purification. 2,2′-azobis (2-methylpropionitrile) (AIBN) (99%, J&K Scientific) was purified by recrystallization in methanol before use. Dimethyl silicone oil (50 cSt, 0.96 g/ml, Sigma-Aldrich) was dried in vacuum at 120°C for 2 h before being mixed with particles.

Fabrication of PIL Particles

The pure PIL (P[VBIm][BF_4]) particles were prepared according to a reference method (Zhang et al., 2017). The monomer [VBIm][BF_4] (3 g) was dispersed in 50 ml of ethanol and was mechanically stirred at 200 rpm for 10 min. Then, PVP (0.22 g) and AIBN (0.08 g) were added to the abovementioned solution. Argon was introduced while mechanically stirring. After 30 min, the mixture was heated in an oil bath at 75°C with mechanical stirring for 12 h. The product was washed with ethanol and water three times and then collected by freeze-drying for 48 h. The composition of the obtained product was determined by ^{1}H-NMR spectroscopy (**Figure 1**). It was found that the three peaks at 7.28 (dd, 1H, CH_2CHN), 5.95 (dd, 2H, CH_2CHN), and 5.43 (dd, 2H, CH_2CHN) corresponding to the vinyl group in the monomer disappeared, indicating that the monomer was successfully polymerized.

[VBIm][BF_4], ^{1}H NMR (400 MHz, DMSO-d_6, δH, ppm): 9.44 (s, 1H, NC*H*N), 8.17 (s, 1H, NC*H*CHN), 7.91 (s, 1H, NCHC*H*N), 7.28 (dd, 1H, CH_2CHN), 5.95 (dd, 2H, CH_2CHN), 5.43 (dd, 2H, CH_2CHN), 4.20 (t, 2H, NCH_2CH_2), 1.81 (m, 2H, NCH_2CH_2), 1.30(h, 2H, $NCH_2CH_2CH_2CH_2$), 0.92 (t, 3H, CH_2CH_3).

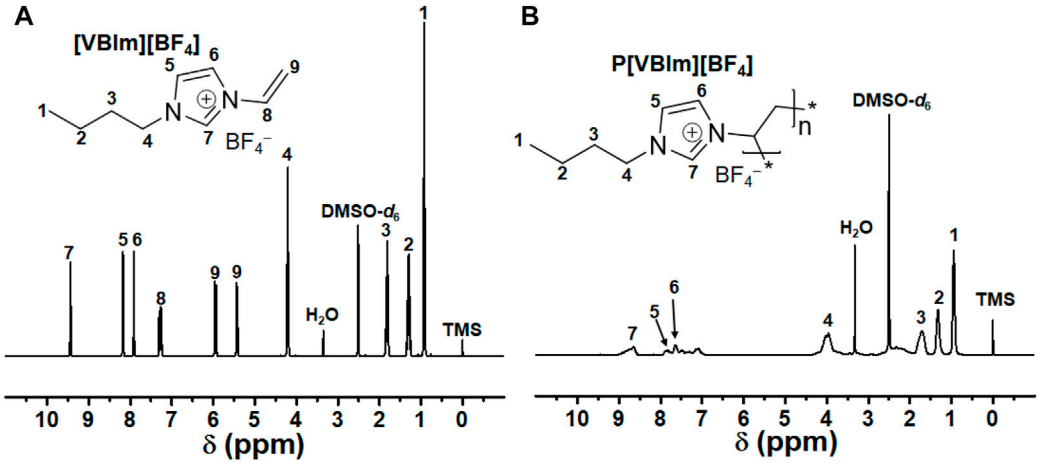

FIGURE 1 | ^{1}H-NMR spectra of IL monomer ([VBIm][BF4]) **(A)** and PIL (P[VBIm][BF4]) **(B)**.

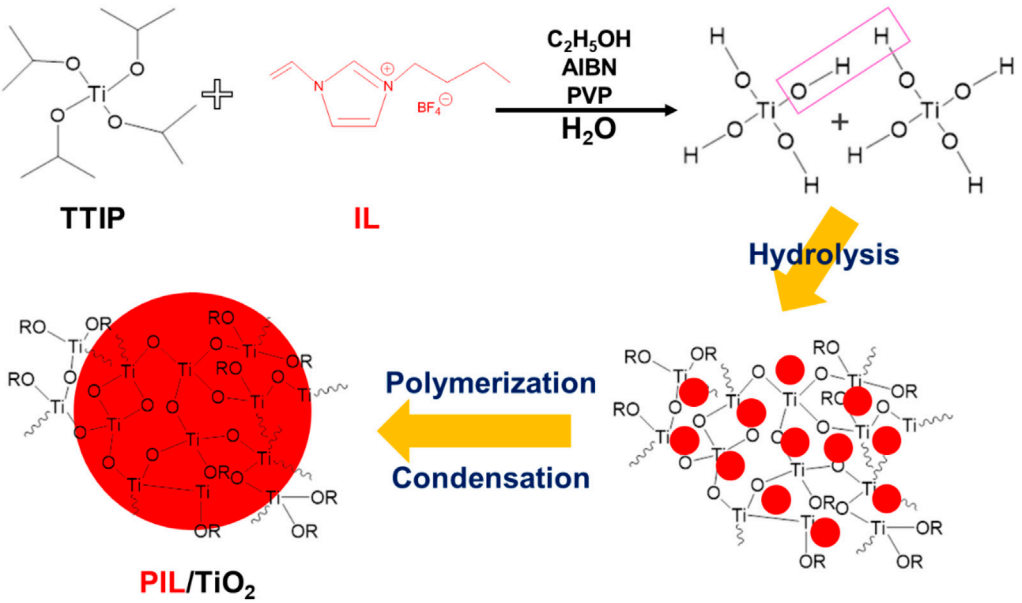

SCHEME 1 | Fabrication process of the PIL/TiO_2 composite.

P[VBIm][BF_4], ^{1}H NMR (400 MHz, DMSO-d_6, δH, ppm): 8.65 (s, 1H, NC*H*N), 7.65 (s, 1H, NC*H*CHN), 7.49 (s, 1H, NCHC*H*N), 3.95 (m, 2H, NCH_2CH_2), 1.71 (s, 2H, NCH$_2$CH_2), 1.33 (m, 2H, NCH$_2$CH$_2$CH_2), 0.94 (d, 3H, CH$_2$CH_3)

One-Pot Fabrication of PIL/TiO_2 Composite Particles

TTIP (3.85 g) and [VBIm][BF_4] (3 g) were dispersed in 50 ml of ethanol, which was mechanically stirred at 200 rpm for 10 min. Then, PVP (0.22 g) and AIBN (0.08 g) were added to the abovementioned solution and mechanically stirred for 20 min. Then, deionized water (2.43 g) was added. Under the protection of argon, the mixture was stirred and heated in an oil bath at 75°C for 12 h. The product was washed with ethanol and water three times and then collected by freeze-drying for 48 h. A schematic process for fabrication of PIL/TiO_2 composite particles is shown in **Scheme 1**.

Characterization

The morphologies of the particles were observed by scanning electron microscopy (SEM) (S4800, Hitachi, Japan) and transmission electron microscopy (TEM) (JEOL 2010; Japan). An energy-dispersive spectroscopy (EDS)–equipped TEM was applied to analyze the elements of the samples. A Fourier infrared spectrometer (FT-IR) (E55 + FRA106, Bruker, Germany) was

applied to determine the chemical structures of the particles. The synthesis of PIL was also confirmed by a ^{1}H nuclear magnetic resonance spectrometer (^{1}H-NMR), (AVANCE-III500, Bruker, Germany). Thermogravimetric analysis (TGA) (STA4993, Netzsch, Germany) was used to study the thermal stability of the samples. Thermal properties of the samples were also examined by diffraction scanning calorimetry (DSC) (2500, TA, United States). An X-ray diffractometer (XRD) (MAX-2500PC, Rigaku, Japan) was applied to analyze the crystal structures of the particles. The density of the fabricated particles was measured by a pycnometer (Micrometrics, AccuPyc1345).

Rheological Measurement

ER fluids (15 vol%) were prepared by dispersing the fabricated PIL and PIL/TiO_2 particles (density for each is 1.37 and 2.08 g/cm^3) in silicone oil. In order to disperse the particles well in silicone oil, mechanical shaking and ultrasonic treatment were applied before rheological measurement. Then, a rotational rheometer (MCR 502, Anton Paar, Austria) was used to measure the rheological properties of the ER fluids. A parallel plate of (PP25/E/Ti) geometry was selected, between which the ER fluid with a thickness of 1 mm was loaded and an electric field was applied. Then, steady and dynamic measurement modes were conducted on the ER fluid to investigate its rheological properties. In the steady-state test, the shear rate was increased from 0.01 to 500 s^{-1}. In addition, in order to explore the electric field responsiveness of the ER fluid, the shear stress curve of the ER fluid was tested under a square-pulsed electric field at a fixed shear rate of 0.1 s^{-1}. In the amplitude sweep tests, the angular frequency was fixed at 10 rad/s in the strain range of 0.001–100%. In the angular frequency sweeps, a fixed strain of 0.003% was applied in the angular frequency range of 1–100 rad/s. For each test, electric field strength was set at a fixed value in the range of 0–4 kV/mm.

RESULTS AND DISCUSSION

Morphologies and Structures

The SEM and TEM images of PIL (P[VBIm][BF_4]) and PIL/TiO_2 composite particles are shown in **Figure 2**. In **Figure 2A**, the PIL particles mainly comprise spherical particles with a broad size distribution ranging from 2.0 to 5.5 μm. Nonspherical particles were also formed, which might be related to the solubility of P[VBIm][BF_4] in ethanol. In **Figure 2B**, the PIL/TiO_2 composite particles are agglomerates formed by a continuous phase with embedded particles of submicron to micron size. The spheres can be seen clearly in the inset of **Figure 2B**, which has a smaller size than the PIL spheres in **Figure 2A**. **Figure 2C** is the TEM image of PIL particles. Both spherical and nonspherical particles are observed. Similar morphologies are shown in **Figure 2D**, the TEM images of PIL/TiO_2 composite particles. The spheres in the composite particles are much smaller than those in the PIL particles shown in **Figure 2C**. In order to further confirm the components of the PIL/TiO_2 particles, back electron diffraction and elemental analysis were carried out. As shown in **Table 1**, it is found that the elements in PIL are C, N, and F, which are the composition of IL. For the PIL/TiO_2 composite, two areas were analyzed. The edge of the nonspherical part (area 1) shows much higher fractions of Ti and O than those shown by the edge of the spherical part (area 2). It means the main chemical of the continuous phase is TiO_2, and the dispersed spheres are PILs. In this mixed reaction system, the hydrolysis of TTIP started immediately when ethanol and water were added. While the polymerization occurred only when the decomposition temperature of the initiator (AIBN) was reached, which means the polymerization started later than hydrolysis. The solution of TiO_2 hindered the growth of PIL such that PIL spheres in the composite are much smaller than pure PIL particles. As the condensation of TiO_2 continues, PIL particles become embedded in the TiO_2 phase.

Figure 3A shows the FT-IR spectra of the IL monomer ([VBIm][BF_4]), PIL (P[VBIm][BF_4]), and PIL/TiO_2. For [VBIm][BF_4], the stretching vibrations of C-H and C-N of the imidazole ring are located at 3155, 1574, and 1176 cm^{-1}, and the stretching vibration of C-H of the vinyl group is located at 3016 cm^{-1}. The FT-IR spectra of the three substances all show a broad peak near 1055 cm^{-1}, which is related to the anionic tetrafluoroborate. By comparison, it is found that the characteristic peak of C-H in the vinyl group at 3016 cm^{-1} disappeared in the spectrum of P (VBIm)(BF_4). It indicates that the ionic monomers have been polymerized successfully. In the spectrum of PIL/TiO_2, both the characteristic peaks of PIL and TiO_2 (800–500 cm^{-1}) can be observed, which confirms the successful synthesis and combination of PIL and TiO_2.

The thermal stability of the IL monomer, pure PIL, and PIL/TiO_2 composite particles was explored by TGA tests, and the results are shown in **Figure 3B**. By comparing the TGA curves of the samples, it is found that the IL monomer and PIL show similar weight loss along with the increase in temperature which means the PIL retains the original thermal stability of the IL very well. The main thermal decomposition zone for both is in the temperature range of 350–450°C. The PIL/TiO_2 composite particles have two weight loss stages in the measured temperature range. The first weight loss occurs between 100 and 200°C, which is caused by the loss of the hydroxyl groups and bound water on the surface of TiO_2 in the composite. The second stage of weight loss is caused by the thermal decomposition of PIL in the range of 350–450°C. Finally, the residual mass of PIL/TiO_2 is 32.79%, which is mostly attributed to TiO_2. Therefore, the mass ratio of PIL to TiO_2 in the composite is about 2:1. **Figure 3C** shows the XRD patterns of PIL and PIL/TiO_2. A broad peak in the same range of 15–30° is observed for the two samples, confirming the amorphous nature of PIL and PIL/TiO_2. In **Figure 3D**, the glass transition temperature (T_g) of the pure PIL and the PIL in the composite is 116 and 170°C, respectively, indicating that the T_g of PIL is improved by the combination with TiO_2.

Electro Responsive Properties

The electroresponsive properties of the pure PIL and the PIL/TiO_2 composite particles in silicone oil were first observed by an optical microscope. **Figure 4** shows the optical micrographs of

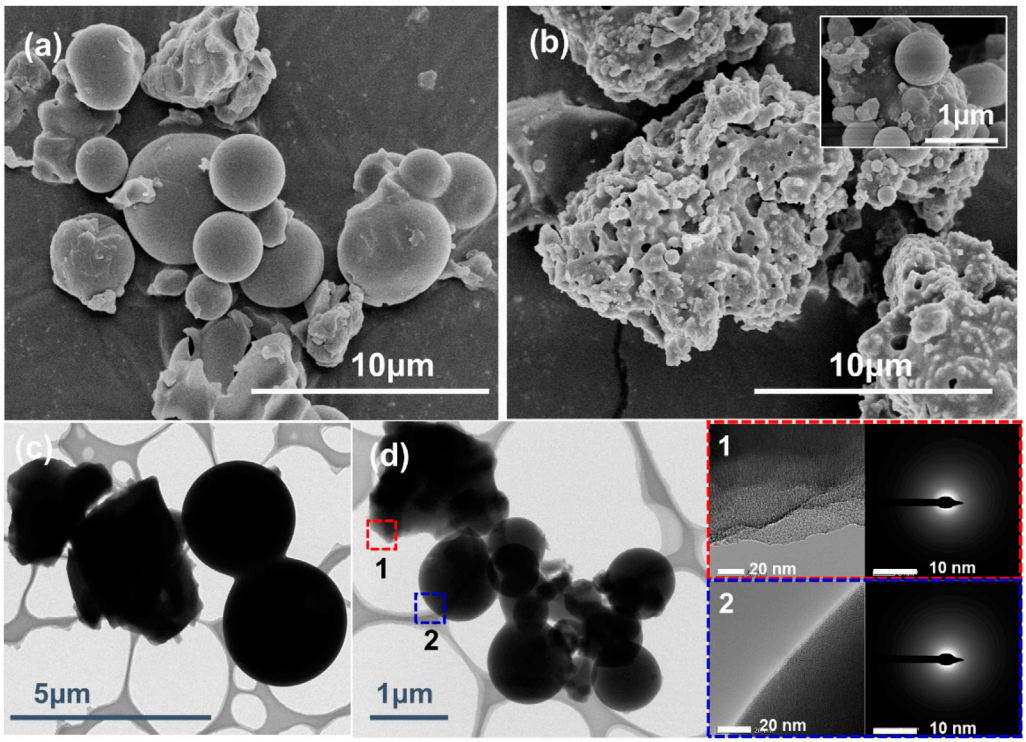

FIGURE 2 | SEM images of PIL **(A)**, PIL/TiO_2 **(B)**, and TEM of PIL **(C)** and PIL/TiO_2 with the electron diffraction pattern of selected parts **(D)**. Inset **(B)** is the SEM image of PIL/TiO_2 particles at a higher magnification.

TABLE 1 | Atomic fraction of the samples determined by EDS analysis.

Sample		Atomic fraction (%)				
		C	N	O	F	Ti
PIL		62.70	6.15	0.00	31.15	0.00
PIL/TiO_2	1	51.71	0.00	13.14	23.58	11.57
	2	63.93	8.80	0.00	25.21	2.06

the fluids of PIL (**Figure 4A**) and PIL/TiO_2 (**Figure 4B**) taken without and with the action of an electric field. Without the effect of an electric field, both kinds of particles dispersed randomly, which quickly agglomerated to form thick chain structures between the electrodes after applying an electric field. That is because the particles were polarized by the electric field and then agglomerated with particles nearby driven by the electrostatic force. The chains formed by the PIL/TiO_2 particles are much denser than those formed by the pure PIL particles, which are related to the morphologies and chemical compositions of the particles.

Figure 5 shows the flow curves of PIL and PIL/TiO_2 ER fluids (15 vol%) at various electric fields. Before the application of an electric field, the two ER fluids both exhibit similar Newtonian fluid characteristics. By contrast, when the electric field strength is increased from 0.5 to 4.0 kV/mm, both fluids exhibit yield stresses, which are needed to make the ER fluids flow under various electric fields. This is due to the fact that has been observed in **Figure 4**: the dispersed particles form dense chain structures between the electrodes. In the entire shear rate range, the two ER fluids both exhibit stable shear stress curves which means the two ER fluids have stable chain structures in the shear rate range. The highlighted difference between the two ER fluids is that the shear stress of PIL/TiO_2 is higher than that of PIL at the same electric field strength. This demonstrates that the combination of TiO_2 with PIL can effectively improve the shear stress value of PIL-based ER fluids.

To further compare the two ER fluids, their yield stresses at each electric field strength were extracted from the flow curves. The shear stress at the beginning of the flow curve is identified as dynamic yield stress (τ_y). The τ_y values of the two ER fluids are plotted in **Figure 6A** as a function of electric field strength (E). It is obvious that the τ_y values of PIL/TiO_2 are significantly higher than those of PIL. The electroresponse of PIL in silicone oil is generated from the local movement of free counter ions at the interface of PIL particles and silicone oil. According to the SEM images of the particles shown in **Figure 2**, the composite particles (containing nearly 66 wt% of PIL and 34 wt% of TiO_2) with irregular shape have a much larger relative surface area, which will improve the interactions between particles. Generally, the relationship between τ_y and electric field strength (E) of ER fluids can be analyzed by a power law equation with a power value (m) in the range of 1–2 (Parthasarathy and Klingenberg, 1996). After fitting using the power law, m equals 1.32 and 1.37, respectively, for PIL and PIL/TiO_2, indicating that the conductivity of the

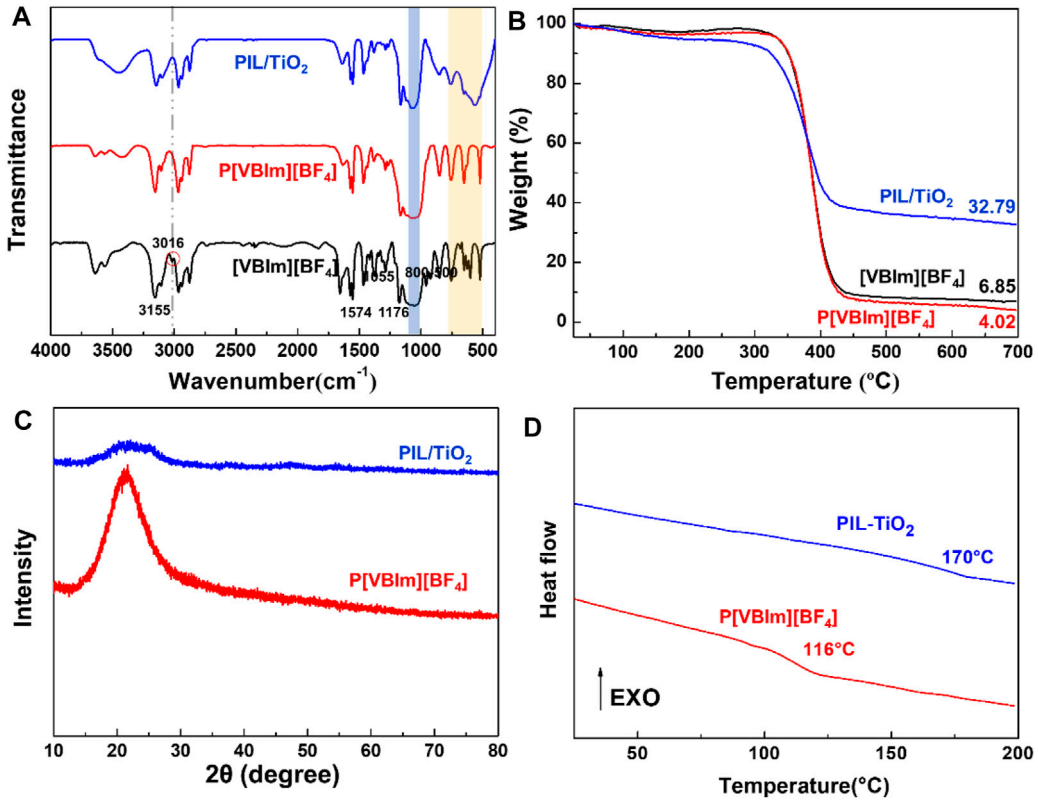

FIGURE 3 | FT-IR spectra **(A)**, TGA curves **(B)**, XRD patterns **(C)**, and DSC curves **(D)** of (VBIm)(BF_4) (IL), P(VBIm)(BF_4) (PIL), and PIL/TiO_2.

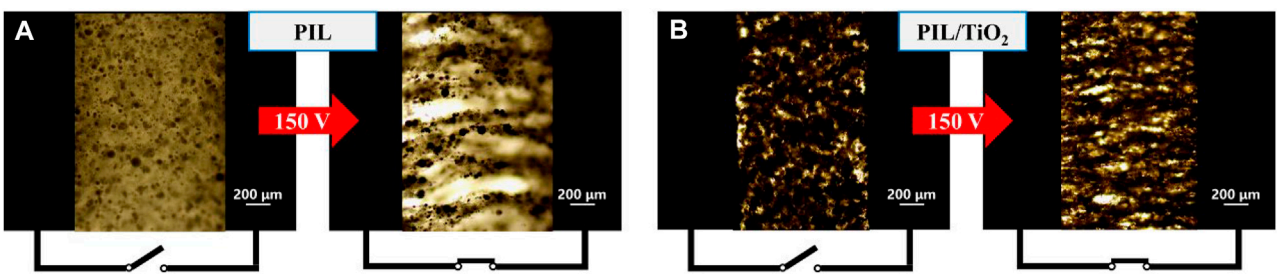

FIGURE 4 | Optical micrograph of the ER fluids (5 vol%) of PIL **(A)** and PIL/TiO_2 **(B)** before and after the application of an electric field (voltage value: 150 V).

particles also plays a significant role in influencing the interaction of particles in electric fields (Wu and Conrad, 1997). The *m* value of the ER fluid of PIL/TiO_2 is larger than that of the PIL particles, which also confirms that the introduction of TiO_2 will improve the electroresponsive properties of PIL.

Figure 6B shows the shear stress curves of PIL and PIL/TiO_2 ER fluids when the electric field is switched on and off alternately under steady shear flow with a fixed shear rate of 0.1 s^{-1}. As shown in the figure, when the electric field is turned on, the shear stress increases rapidly and forms a stable platform area. When the electric field is turned off, the chain structure loses its strength at the electric field and will be quickly destroyed under the action of the shear flow, thus exhibiting very low shear stress approaching zero. Similar to the flow curves shown in **Figure 5**, the shear stress of the ER fluids at pulsed electric fields also increases with the increase of electric field strength, and the shear stress of PIL/TiO_2 is higher than that of PIL at the same electric field strength. In addition, it is also found that the switching effect of the ER fluids is fast and repeatable, which is necessary for electrically controlled devices.

Figures 7A–D show the dynamic sweep curves of the ER fluids of PIL and PIL/TiO_2. In each figure, the storage and loss modulus (G' and G'') are plotted as a function of stain or angular frequency. G' and G'' of the ER fluids imply their solid-like properties. In the amplitude sweep tests (**Figures 7A,B**), under zero field, the two ER fluids show liquid-like behavior with very low G' and G'' in the

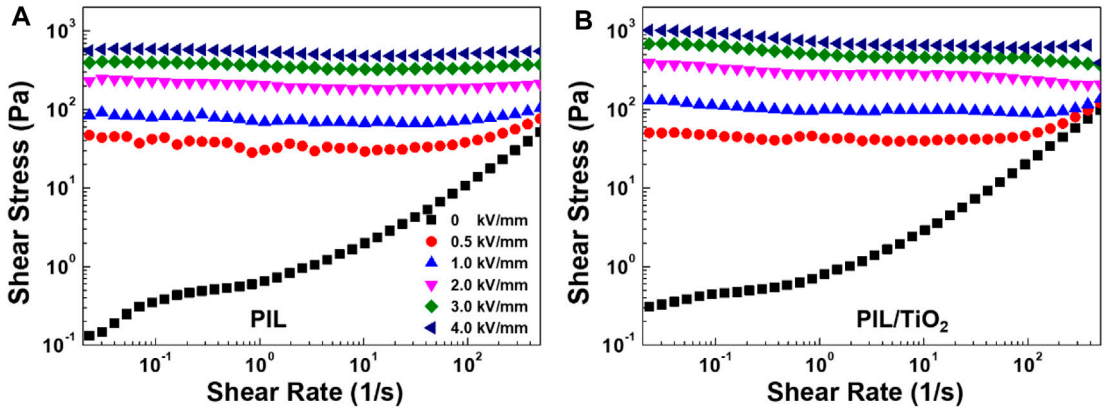

FIGURE 5 | Shear stress curves as a function of the shear rate of the ER fluids of PIL **(A)** and PIL/TiO_2 **(B)** at 25°C under various electric field strengths.

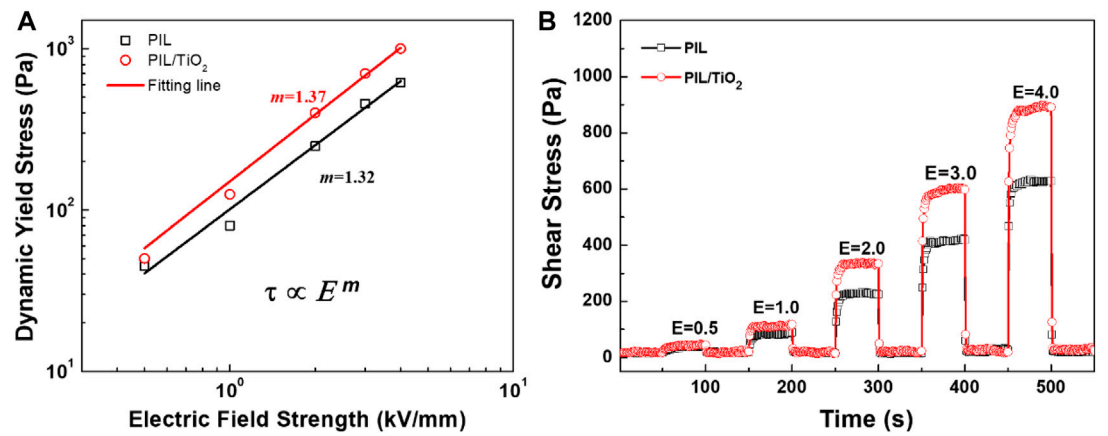

FIGURE 6 | Dynamic yield stress of the ER fluids as a function of electric field strength **(A)** and shear stress of the ER fluids at a square pulsed electric field (unit: kV/mm) **(B)**.

entire strain range; however, under the action of an electric field (E = 0.5–4.0 kV/mm), they show enormously increased G′ which can be 10^5 Pa at E = 4.0 kV/mm. At each applied electric field strength, G′ is much higher than G″ and shows a stable plateau region when the critical strain is not reached, which indicates the solid nature of each ER fluid. When the applied strain is over the critical value, G′ starts to decrease, which means the particle chains are destroyed by the large strain. The strain range before the critical value is called the viscoelastic region of the ER fluid. Comparing the two figures shown by PIL and PIL/TiO_2, it is found that the plateau value of G′ for PIL/TiO_2 is much higher than that of PIL, which means at the same electric field, the PIL/TiO_2 ER fluid has stronger rigidity than PIL ER fluid.

Figures 7C,D show the angular frequency sweep curves of the ER fluids of PIL and PIL/TiO_2 measured under a fixed strain in the viscoelastic range. In the absence of an electric field, G′ and G″ of each ER fluid have similar value in a very low level (10–100 Pa), indicating that the interactions between particles are weak. When an electric field is applied, the values of G′ are in the range of 10^4–10^6 Pa, much higher than those of G″ because of the formation of robust particle chains in the ER fluids. The strength of the chains increases with the increasing of E such that G′ increases with E as well. In addition, both G′ and G″ values of the PIL/TiO_2 ER fluid are much higher than those of the PIL ER fluid, confirming the higher ER effect of the composite particles.

Figure 8 shows the yield stress of the ER fluids measured at different temperatures. As we know, when temperature increases, the viscosity of silicone oil decreases which means the shear stress of the ER fluids at zero electric field strength will decrease. Differently, as an electric field is applied, an increase in shear stress might be observed with the increase in temperature. It is because at higher temperatures, more chemicals in the particles can be polarized, which means the interactions between particles increase. Unfortunately, the mobility of anions in PIL is also improved by increasing temperature so that leakage current rises rapidly until a short circuit occurs at critical electric field strength. For the ER fluid of PIL, the operation temperature decreases obviously with the increase of applied electric field strength. Because of the enhancement of ion mobility in pure PIL, the highest operation temperature is 60°C at E = 3 kV/mm because of

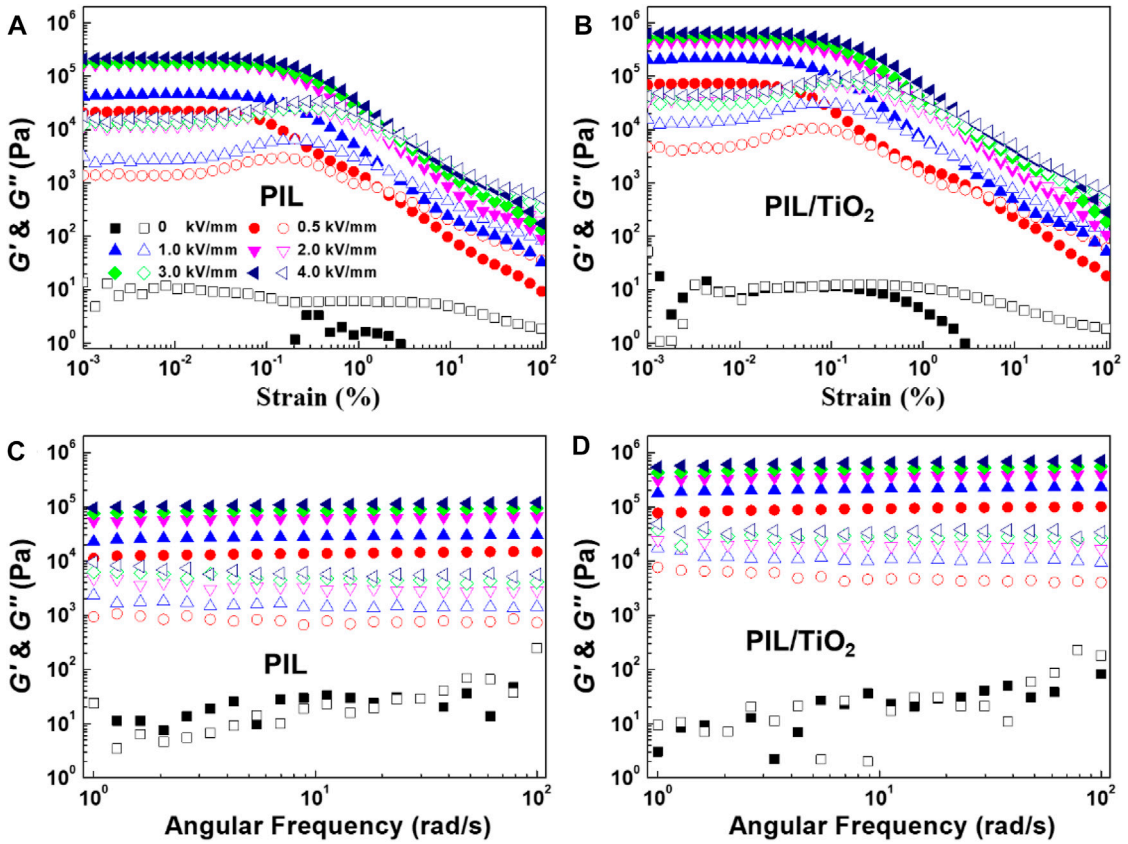

FIGURE 7 | Amplitude **(A,B)** and angular frequency **(C,D)** sweep curves of the ER fluids of PIL **(A,C)** and PIL/TiO_2 **(B,D)** at 25°C under different electric field strengths.

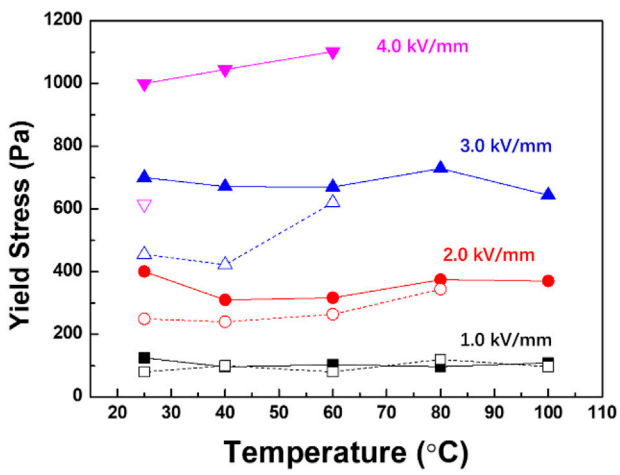

FIGURE 8 | Yield stress of the ER fluids of PIL (open) and PIL/TiO_2 (solid) as a function of temperature at different electric field strengths.

the enhancement of ion mobility in pure PIL; by contrast, it is 100°C for the PIL/TiO_2 ER fluid. It indicates that the composite particles are more stable than pure PIL particles at higher temperature, which is attributed to the continuous inorganic TiO_2 phase that limits the movement of anions of PIL. The significant improvement of T_g of PIL in the PIL/TiO_2 composite, which has been shown in **Figure 3D**, also confirms the restriction of TiO_2 on the movement of PIL chains.

CONCLUSION

PIL-based composite particles, PIL/TiO_2, were fabricated by a facile one-pot method by combining the polymerization of IL monomer and the hydrolysis of titanate in one system. Morphological analysis proved that in the irregularly shaped composite particles, PIL micron spheres were embedded in the continuous TiO_2 phase. The PIL spheres in the composite were not as big as those fabricated in a single polymerization process, which demonstrated that the sol solution of TiO_2 influenced the growth of the PIL spheres. TGA results indicated that the mass ratio of PIL to TiO_2 in the composite particle was 2:1. Steady and dynamic rheological analysis revealed that the PIL/TiO_2 ER fluid had higher yield stress and higher storage modulus at electric fields. More importantly, the PIL/TiO_2 ER fluid can work at high temperatures up to 100°C at E = 3.0 kV/mm, which is

much higher than that of pure PIL ER fluid (60°C). The one-pot fabricated PIL/TiO_2 suggested a facile way to prepare PIL-based composite particles for the research of electroresponsive materials with excellent responsiveness and a broad working temperature range.

DATA AVAILABILITY STATEMENT

The original contributions presented in the study are included in the article/Supplementary Material; further inquiries can be directed to the corresponding author.

AUTHOR CONTRIBUTIONS

GZ performed the experiments and drafted the initial manuscript. SY, ZZ, CD, and XJ assisted in the experiment. L-MW and YL supervised the research and revised the manuscript.

FUNDING

This work was supported by the National Natural Science Foundation of China (Grant no. 21872118) and the Youth Top Talent Support Program of Hebei Province.

REFERENCES

Agrawal, N., and Sharma, S. C. (2021). Effect of the ER Lubricant Behaviour on the Performance of Spherical Recessed Hydrostatic Thrust Bearing. *Tribology Int.* 153, 106621. doi:10.1016/j.triboint.2020.106621

Armand, M., Endres, F., MacFarlane, D. R., Ohno, H., and Scrosati, B. (2009). Ionic-Liquid Materials for the Electrochemical Challenges of the Future. *Nat. Mater* 8, 621–629. doi:10.1038/nmat2448

Bitman, L., Choi, Y. T., Choi, S. B., and Wereley, N. M. (2004). Electrorheological Damper Analysis Using an Eyring-Plastic Model. *Smart Mater. Struct.* 14, 237–246. doi:10.1088/0964-1726/14/1/024

Chen, G.-Y., Chang, C.-J., Lu, C.-H., and Chen, J.-K. (2020). Electrorheological Display Loading Medium of Core/shell Polystyrene/polyvinyltetrazole Microspheres for On-Site Visualization of Lead(II). *Polymer* 203, 122805. doi:10.1016/j.polymer.2020.122805

Delgado-Canto, M. A., Fernández-Silva, S. D., Roman, C., and García-Morales, M. (2020). On the Electro-Active Control of Nanocellulose-Based Functional Biolubricants. *ACS Appl. Mater. Inter.* 12, 46490–46500. doi:10.1021/acsami.0c12244

Dong, Y., Yin, J., and Zhao, X. (2014). Microwave-synthesized Poly(ionic Liquid) Particles: a New Material with High Electrorheological Activity. *J. Mater. Chem. A.* 2, 9812–9819. doi:10.1039/c4ta00828f

Earle, M. J., and Seddon, K. R. (2000). Ionic Liquids. Green Solvents for the Future. *Pure Appl. Chem.* 72, 1391–1398. doi:10.1351/pac200072071391

Gao, M. R., Yuan, J., and Antonietti, M. (2017). Ionic Liquids and Poly(ionic Liquid)s for Morphosynthesis of Inorganic Materials. *Chem. Eur. J.* 23, 5391–5403. doi:10.1002/chem.201604191

Halsey, T. C. (1992). Electrorheological Fluids. *Science* 258, 761–766. doi:10.1126/science.258.5083.761

Hao, T., Xu, Z., and Xu, Y. (1997). Correlation of the Dielectric Properties of Dispersed Particles with the Electrorheological Effect. *J. Colloid Interf. Sci.* 190, 334–340. doi:10.1006/jcis.1997.4871

He, F., Xue, B., Lei, Q., Liu, Y., Zhao, X., and Yin, J. (2021). Influence of Molecular Weight on Electro-Responsive Electrorheological Effect of Poly(ionic Liquid)s: Rheology and Dielectric Spectroscopy Analysis. *Polymer* 234, 124241. doi:10.1016/j.polymer.2021.124241

Jang, H. S., Kwon, S. H., Lee, J. H., and Choi, H. J. (2019). Facile Fabrication of Core-Shell Typed Silica/poly(diphenylamine) Composite Microparticles and Their Electro-Response. *Polymer* 182, 121851. doi:10.1016/j.polymer.2019.121851

Kikuchi, T., Abe, I., NagataYamaguchi, T. A., Yamaguchi, A., and Takano, T. (2020). Twin-driven Actuator with Multi-Layered Disc Magnetorheological Fluid Clutches for Haptics. *J. Intell. Mater. Syst. Structures* 32, 1326–1335. doi:10.1177/1045389x20943958

Kovaleva, V. V., Kuznetsov, N. M., Istomina, A. P., Bogdanova, O. I., Vdovichenko, A. Y., Streltsov, D. R., et al. (2022). Low-filled Suspensions of α-chitin Nanorods for Electrorheological Applications. *Carbohydr. Polym.* 277, 118792. doi:10.1016/j.carbpol.2021.118792

Lee, S., Kim, Y. K., Hong, J.-Y., and Jang, J. (2016). Electro-response of MoS2 Nanosheets-Based Smart Fluid with Tailorable Electrical Conductivity. *ACS Appl. Mater. Inter.* 8, 24221–24229. doi:10.1021/acsami.6b07887

Lei, Q., Zheng, C., He, F., Zhao, J., Liu, Y., Zhao, X., et al. (2018). Enhancing Electroresponsive Electrorheological Effect and Temperature Dependence of Poly(ionic Liquid) Particles by Hard Core Confinement. *Langmuir* 34, 15827–15838. doi:10.1021/acs.langmuir.8b03508

Liang, Y., Yuan, X., Wang, L., Zhou, X., Ren, X., Huang, Y., et al. (2020). Highly Stable and Efficient Electrorheological Suspensions with Hydrophobic Interaction. *J. Colloid Interf. Sci.* 564, 381–391. doi:10.1016/j.jcis.2019.12.129

Liu, Y., Davidson, R., and Taylor, P. (2005). Touch Sensitive Electrorheological Fluid Based Tactile Display. *Smart Mater. Struct.* 14, 1563–1568. doi:10.1088/0964-1726/14/6/049

Liu, Y., Zhao, J., He, F., Zheng, C., Lei, Q., Zhao, X., et al. (2019a). Ion Transport, Polarization and Electro-Responsive Elelctrorheological Effect of Self-Crosslinked Poly(ionic Liquid)s with Different Counterions. *Polymer* 177, 149–159. doi:10.1016/j.polymer.2019.05.071

Liu, Y., Zhao, J., He, F., Zheng, C., Zhao, X., and Yin, J. (2019b). Influence of Alkyl Spacer Length on Ion Transport, Polarization and Electro-Responsive Electrorheological Effect of Self-Crosslinked Poly(ionic Liquid)s. *Polymer* 171, 161–172. doi:10.1016/j.polymer.2019.03.053

Liu, Z., Chen, P., Jin, X., Wang, L.-M., Liu, Y., and Choi, H. (2018). Enhanced Electrorheological Response of Cellulose: A Double Effect of Modification by Urea-Terminated Silane. *Polymers* 10, 867. doi:10.3390/polym10080867

Lu, Q., Han, W., and Choi, H. (2018). Smart and Functional Conducting Polymers: Application to Electrorheological Fluids. *Molecules* 23, 2854. doi:10.3390/molecules23112854

Marins, J. A., Soares, B. G., Silva, A. A., Hurtado, M. G., and Livi, S. (2013). Electrorheological and Dielectric Behavior of New Ionic Liquid/silica Systems. *J. Colloid Interf. Sci.* 405, 64–70. doi:10.1016/j.jcis.2013.05.013

Parthasarathy, M., and Klingenberg, D. (1996). Electrorheology: Mechanisms and Models. *Mater. Sci. Eng. R: Rep.* 17, 57–103. doi:10.1016/0927-796X(96)00191-X

Plachy, T., Sedlacik, M., Pavlinek, V., and Stejskal, J. (2015). The Observation of a Conductivity Threshold on the Electrorheological Effect of P-Phenylenediamine Oxidized with P-Benzoquinone. *J. Mater. Chem. C* 3, 9973–9980. doi:10.1039/c5tc02119g

Qiu, Z., Shen, R., Huang, J., Lu, K., and Xiong, X. (2019). A Giant Electrorheological Fluid with a Long Lifetime and Good thermal Stability Based on TiO2 Inlaid with Nanocarbons. *J. Mater. Chem. C* 7, 5816–5820. doi:10.1039/c9tc00364a

Schwarz, G., Maisch, S., Ullrich, S., Wagenhöfer, J., and Kurth, D. G. (2013). Electrorheological Fluids Based on Metallo-Supramolecular Polyelectrolyte-Silicate Composites. *ACS Appl. Mater. Inter.* 5, 4031–4034. doi:10.1021/am401104d

Sun, W., Zheng, H., Chen, Y., Li, C., Wang, B., Hao, C., et al. (2021). Preparation and Electrorheological Properties of Peanut-Like Hollow Core-Shell Structure TiO 2 @SiO 2 Nanoparticles. *Adv. Eng. Mater.* 23, 2001416. doi:10.1002/adem.202001416

Sun, Y., Huang, Y., Wang, M., Wu, J., Yuan, S., Ding, J., et al. (2020). Design, Testing and Modelling of a Tuneable GER Fluid Damper under Shear Mode. *Smart Mater. Struct.* 29, 085011. doi:10.1088/1361-665X/ab914a

Wen, Q., Ma, L., Wang, C., Wang, B., Han, R., Hao, C., et al. (2019). Preparation of Core-Shell Structured Metal-Organic Framework@PANI Nanocomposite and

its Electrorheological Properties. *RSC Adv.* 9, 14520–14530. doi:10.1039/C9RA02268F

Wen, W., Huang, X., Yang, S., Lu, K., and Sheng, P. (2003). The Giant Electrorheological Effect in Suspensions of Nanoparticles. *Nat. Mater* 2, 727–730. doi:10.1038/nmat993

Wu, C. W., and Conrad, H. (1997). Dielectric and Conduction Effects in Non-ohmic Electrorheological Fluids. *Phys. Rev. E* 56, 5789–5797. doi:10.1103/PhysRevE.56.5789

Wu, J., Song, Z., Liu, F., Guo, J., Cheng, Y., Ma, S., et al. (2016). Giant Electrorheological Fluids with Ultrahigh Electrorheological Efficiency Based on a Micro/nano Hybrid Calcium Titanyl Oxalate Composite. *NPG Asia Mater.* 8, e322. doi:10.1038/am.2016.158

Zhang, G., Zhao, X., Jin, X., Zhao, Z., Ren, Y., Wang, L.-M., et al. (2021). Ionic-liquid-modified TiO2 Spheres and Their Enhanced Electrorheological Responses. *J. Mol. Liquids* 338, 116696. doi:10.1016/j.molliq.2021.116696

Zhang, W. L., and Choi, H. J. (2014). Graphene Oxide Based Smart Fluids. *Soft Matter* 10, 6601–6608. doi:10.1039/c4sm01151a

Zhang, W. L., Wei, W., Liu, W., Guan, T., Tian, Y., and Zeng, H. (2019). Engineering the Morphology of TiO2/carbon Hybrids via Oxidized Ti3C2Tx MXene and Associated Electrorheological Activities. *Chem. Eng. J.* 378, 122170. doi:10.1016/j.cej.2019.122170

Zhang, Z., Zhang, Z., Hao, B. N., Zhang, H., Wang, M., and Liu, Y. D. (2017). Fabrication of Imidazolium-Based Poly(ionic Liquid) Microspheres and Their Electrorheological Responses. *J. Mater. Sci.* 52, 5778–5787. doi:10.1007/s10853-017-0812-4

Zhao, J., Lei, Q., He, F., Zheng, C., Liu, Y., Zhao, X., et al. (2019). Interfacial Polarization and Electroresponsive Electrorheological Effect of Anionic and Cationic Poly(ionic Liquids). *ACS Appl. Polym. Mater.* 1, 2862–2874. doi:10.1021/acsapm.9b00565

Zhao, J., Liu, Y., Zheng, C., Lei, Q., Dong, Y., Zhao, X., et al. (2018). Pickering Emulsion Polymerization of Poly(ionic Liquid)s Encapsulated Nano-SiO2 Composite Particles with Enhanced Electro-Responsive Characteristic. *Polymer* 146, 109–119. doi:10.1016/j.polymer.2018.05.030

Zhao, X. P., and Yin, J. B. (2002). Preparation and Electrorheological Characteristics of Rare-Earth-Doped TiO2 Suspensions. *Chem. Mater.* 14, 2258–2263. doi:10.1021/cm011522w

Zhao, Y., Liu, X., Fang, Y., and Cao, C. (2021). Ultra-Precision Processing of Conductive Materials via Electrorheological Fluid-Assisted Polishing. *Adv. Eng. Mater.* 23, 2001109. doi:10.1002/adem.202001109

Zhao, Z., Zhang, G., Yin, Y., Dong, C., and Liu, Y. D. (2020). The Electric Field Responses of Inorganic Ionogels and Poly(ionic Liquid)s. *Molecules* 25, 4547. doi:10.3390/molecules25194547

Conflict of Interest: The authors declare that the research was conducted in the absence of any commercial or financial relationships that could be construed as a potential conflict of interest.

Publisher's Note: All claims expressed in this article are solely those of the authors and do not necessarily represent those of their affiliated organizations, or those of the publisher, the editors, and the reviewers. Any product that may be evaluated in this article, or any claim that may be made by its manufacturer, is not guaranteed or endorsed by the publisher.